Optimising oscillating waveform-shape for pore size sensitivity in diffusion-weighted MR

Ivana Drobnjak *, Gastao Cruz, Daniel C. Alexander

Center for Medical Image Computing, Department of Computer Science, University College London (UCL), Gower Street, London WC1E 6BT, UK

ARTICLE INFO

ABSTRACT

Optimising the shape of a generalised gradient waveform (GEN) in diffusion-weighted MR has been shown to, in theory, greatly increase sensitivity to pore size. The broad class of optimised shapes takes simple oscillatory forms. To speed up convergence of the optimisation, improve computation times and make the waveforms more practical, here we explore various oscillatory waveforms constructed from trapezoidal and sinusoidal shapes and compare their performance with the optimised GEN waveform. The oscillating waveforms are optimised to maximise sensitivity to parameters, such as axon radius, intra-cellular volume fraction and diffusion constants, of a simple white matter model. Simulation experiments find that all oscillating waveforms we tried perform significantly better than the original generalised waveform due to the improved convergence of the optimisation. Differences among the oscillating shapes however are very small and although a truncated sinusoidal waveform consistently gives the lowest cost function, no significant difference in the estimated model parameters was found. Therefore the simplest choice, i.e. the trapezoidal parametrisation, seems sufficient for most practical purposes.

1. Introduction

Diffusion-weighted Magnetic Resonance (MR) can provide insight into pore morphology and fluid transport [1] and is therefore useful for studying porous structures such as sandstone rocks, catalysts or biological tissues [2–4]. Here, we focus on biomedical imaging where diffusion MRI offers the potential to map microstructural features in tissue [5–7]. More specifically, we look into the potential to image axon radius in the white matter, which is a key challenge as axon radius affects nerve function and hence a reliable technique could provide new insight into various neuronal diseases [8,9].

The shape of the diffusion gradient waveform in diffusion MRI pulse sequences affects the sensitivity of diffusion MRI signal to the microstructure [10,11,7,12]. Previously we have shown that optimised generalised gradient waveforms (GEN) provide much better sensitivity to pore sizes than rectangular pulses such are those in standard diffusion sequences [11,13]. This is because the optimisation in [11,13] discretises a general waveform and varies each point independently. Thus the search space is high-dimensional (hundreds of degrees of freedom) so convergence to the optimal configuration is slow and in practice the global minimum is difficult to find.

Here we look for a simple parametrized gradient waveform defined with just a few parameters that would produce results of similar quality to the optimised GEN results. So far we found that optimised GEN solutions [11,13] consistently approach simple oscillatory forms, but it is not clear what exact shapes they have or whether departures from simple oscillations are important. To improve the convergence and gain a better understanding of the ideal oscillating shape, here we run similar optimisations using parametrized oscillating waveforms with various shapes such as trapezoidal and sinusoidal, and compare their performance in simulation.

2. Methods

2.1. Tissue model

We assume a simple white matter tissue model [10] with straight parallel non-abutting cylindrical axon cells, with equal radii and impermeable walls embedded in a homogenous extra-cellular medium. The parameters of the model are: the volume fraction $f \in [0, 1]$ of the intra cellular compartment; the axon direction $\mathbf{n}$; the axon radius R; the intrinsic diffusion coefficient $D_\parallel$; and the apparent diffusion coefficient $D_\perp$. In the extracellular space the diffusion is hindered and modelled with a diffusion tensor $(D_\parallel - D_\perp)\mathbf{nn}^T + D_\perp\mathbf{I}$, which has a major eigenvector $\mathbf{n}$ in the fiber direction with corresponding eigenvalue $D_\parallel$ (the diffusivity parallel

* Corresponding author. Tel.: +44 (0)20 3108 1061; fax: +44 (0)20 7387 1397.
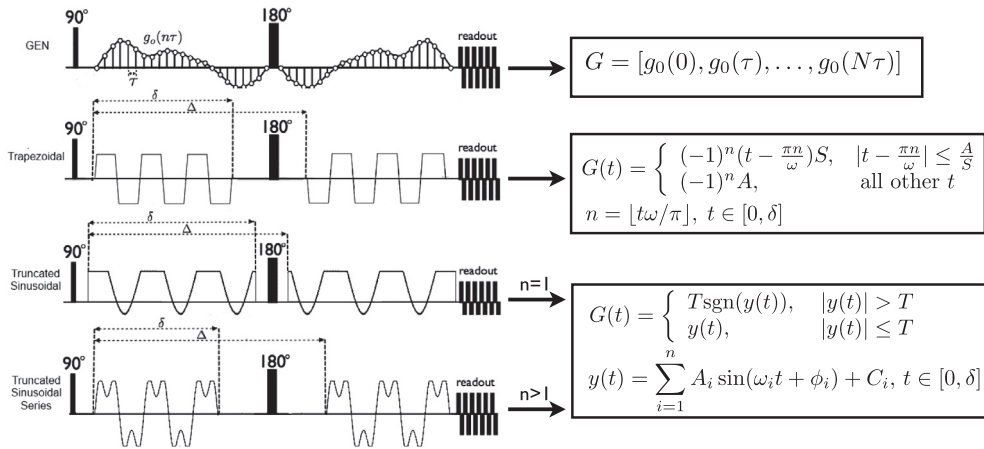*E-mail address:* i.drobnjak@ucl.ac.uk (I. Drobnjak).

Fig. 1. On the left a diagram of the various parametrisations tested. On the right are the functions *G* describing the shape before the 180° RF pulse. The second half is mirrored. Function sgn is the regular sign function.
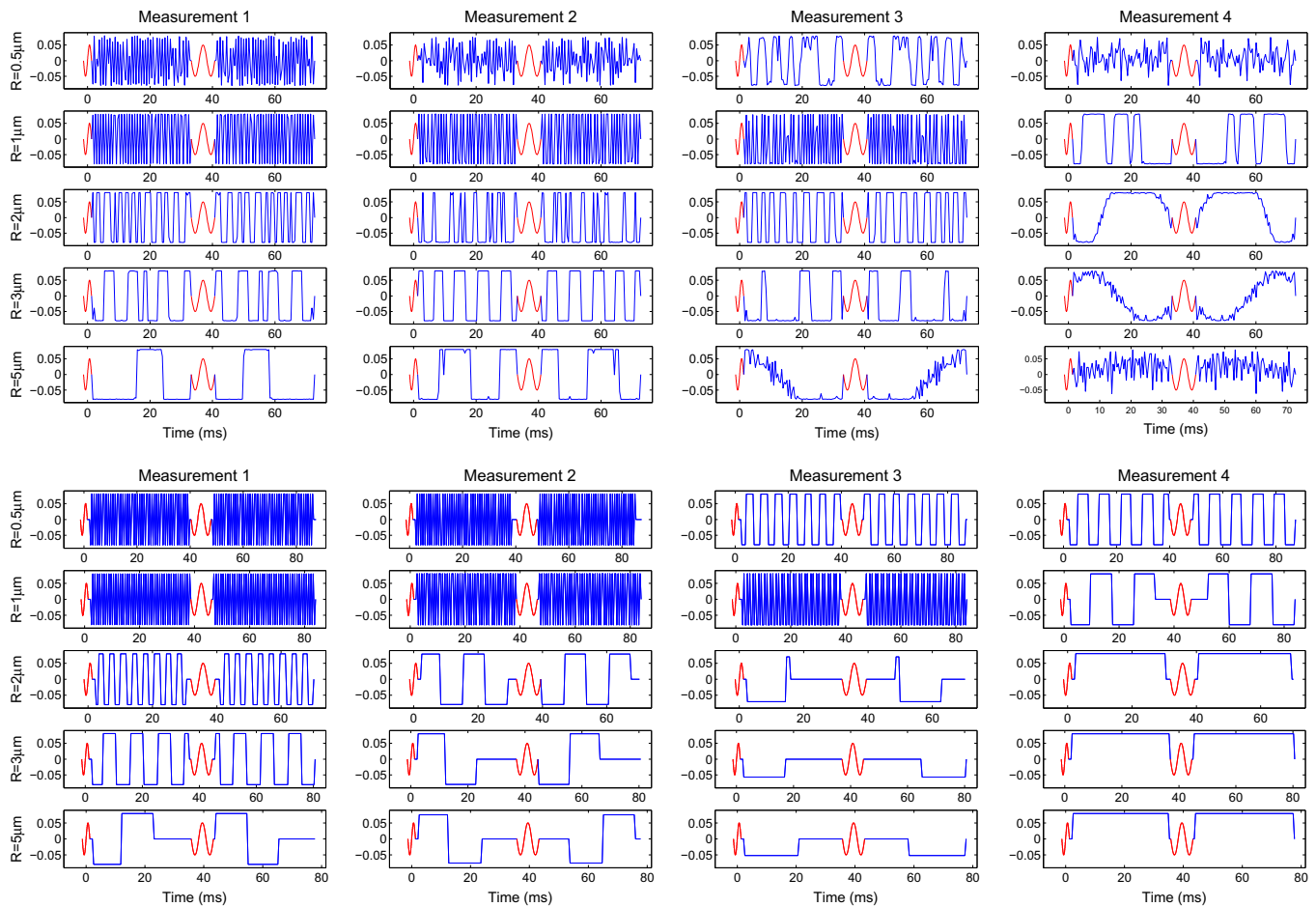

Fig. 2. Optimised GEN (top) and trapezoidal (bottom) waveforms.

to **n**) and minor eigenvalues $D_\perp$ (the apparent diffusivity perpendicular to **n**); **I** is the identity tensor. The intracellular space has a single intrinsic (i.e. short time limit) diffusion coefficient $D_\parallel$ (the time dependent apparent diffusivity emerges from the model of restriction in the intracellular space).

2.2. Signal model

The diffusion MR signal is calculated as a linear combination of normalised MR signals coming from restricted intra-cellular diffus-

ing particles and hindered extra-cellular diffusing particles with a Gaussian displacement distribution. To estimate the diffusion signal from the restricted compartment we use the matrix formalism [14,11,15].

2.3. Pulse sequence model

The pulse sequence model has the same basic structure as the generalised waveform (GEN) sequence [11], with parametrized oscillating waveforms in place of the discretely defined generalised

Table 1
Cost function values for a range of radii. Best (lowest) results present in bold.

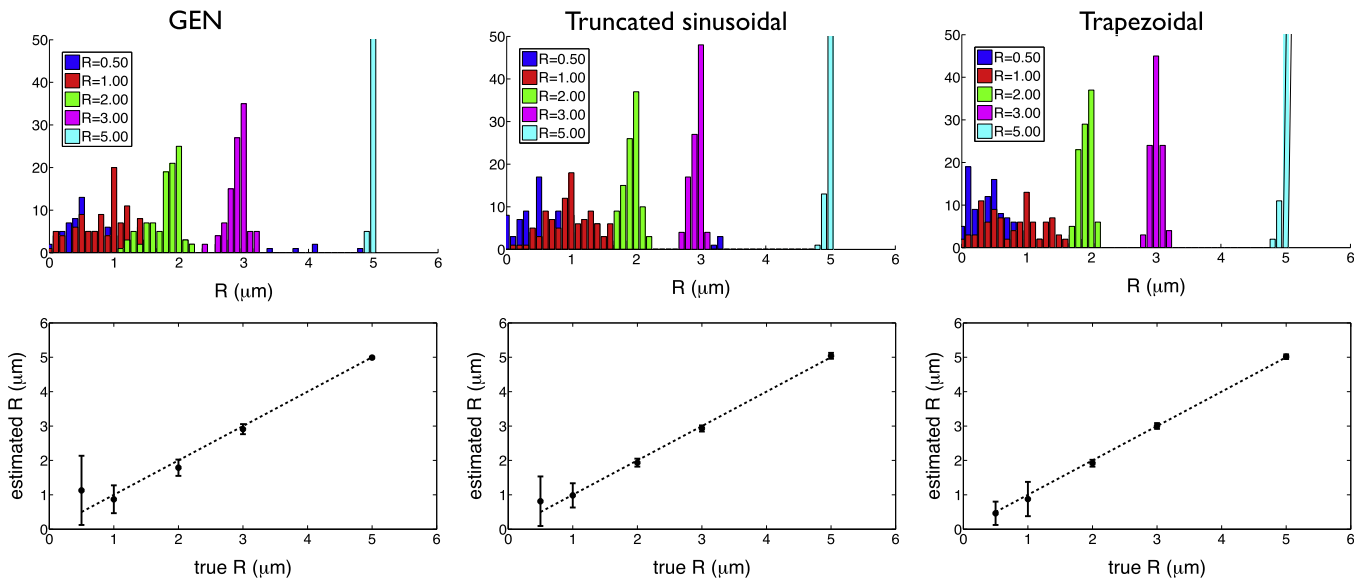| Parametrization	$R = 0.5\ \mu m$	$R = 1\ \mu m$	$R = 2\ \mu m$	$R = 3\ \mu m$	$R = 5\ \mu m$
GEN	8.57E + 009	3.12E + 003	71.2	4.84	0.341
Trapezoidal	4.06E + 009	2.74E + 003	27.6	1.05	0.140
Truncated Sinusoidal	3.66E + 009	**2.59E + 003**	21.3	**0.800**	**0.121**
Truncated Sinusoidal series ($n = 2$)	**3.62E + 009**	2.61E + 003	**20.0**	0.882	0.122
Truncated Sinusoidal series ($n = 3$)	4.37E + 009	2.72E + 003	21.4	0.922	0.127

Fig. 3. Axon radius estimation for optimised GEN and parametrized protocols. The top diagrams represent the posterior distributions. The bottom diagrams represent the mean and the standard deviation of the estimates. The dotted line represents the true value of the axon radius.

waveforms as Fig. 1 illustrates. All waveforms are mirrored about the 180° degree pulse and are constrained not to violate pre-defined maximum gradient strength G_{max} and slew rate S. Optimised parameters are: GEN – amplitudes $g_0(0), g_0(\tau), \ldots, g_0(N\tau)$ and the number of points N ($N > 80$ in most cases); Trapezoidal – amplitude A, frequency ω, duration δ, time interval between the onset of the first and the second waveform Δ; Truncated sinusoidal series – A_i, ω_i, phase ϕ_i, constant C_i, truncation T, δ, Δ where $i = 1 \ldots n$ and n is the number of waveforms in the series ($n = 1$ for Truncated Sinusoidal).

3. Results and discussion

The optimisation proceeds as in [11] for various cylinder radii. Each produces a protocol of four pulse sequences (measurements). We then synthesise data from each, add Rician noise, and estimate the posterior distributions using the Markov Chain Monte Carlo method, as in [10,11], to compare the parameter estimate precision each protocol provides. The simulation experiments here use a gradient system with $G_{max} = 0.08$ T/m and slew rate $S = 400$ T/m/s, but the main findings are independent of these choices.

Fig. 2 presents optimised protocols for the GEN (top) and trapezoidal waveform (bottom). Each row corresponds to a different radius R, and shows the four measurements for that R. The optimised trapezoidal waveforms follow the frequency and the amplitude trend of the GEN waveforms. However, the trapezoidal parametrisation avoids the noisy features in the GEN waveforms. Optimised truncated sinusoidal waveforms (not shown) produce protocols with similar combinations of frequency and amplitude. Table 1 shows the minimum value of the optimised objective function F as a function of radius R for each parametrization. The smal-

ler search space for the parametrized oscillating waveforms allows the optimisation to find solutions with three times lower values of F than for GEN even though GEN can take the form of any of the oscillating waveform-shapes. Truncated Sinusoids with $n = 1$ or 2 consistently produce the lowest F. As n increases the value of F goes up because the search space becomes high-dimensional hindering convergence. While cost function values are informative, they summarise sensitivity to all parameters so it is unclear where the advantages arise from. Fig. 3 shows posterior distributions on radius R for GEN, trapezoidal and truncated sinusoidal waveforms. The posterior distributions are narrower for the parametrized oscillatory protocols, demonstrating higher precision in estimating the radius than the GEN protocols. The bottom row of the figure confirms that the parametrized gradients sequences produce more accurate (closer to the diagonal) and precise (smaller error bars) estimates compared to GEN. The optimised trapezoidal and truncated sinusoidal waveforms have similar precision and accuracy.

Although we show only a few examples we have looked at various intermediate waveforms e.g. waveform constants C_i and/or ω fixed to zero. All produce similar results to the waveforms shown, with slightly higher cost function than the truncated sinusoid shape.

4. Conclusion

Protocols of simple oscillating waveform-shapes optimised for pore size estimation via a simple white matter model produce similar components of frequency and amplitude as GEN protocols. The objective function values are markedly lower for the optimised oscillation shapes due to the reduction in the dimensionality of the search space (from hundreds to tens). The oscillating protocols show only minor differences: although the truncated sinusoidal

waveform gives the lowest cost function, no significant difference in the estimated model parameters was found.

We suggest based on these results that the simplest optimised oscillating shape, i.e. trapezoidal, is sufficient for most practical purposes. It enables simple and efficient approximation of the restricted diffusion signal e.g. by using Gaussian Phase Distribution approximation of the diffusion signal [16], hence allowing for fast and efficient model parameter fitting. All optimized gradient waveforms we presented here can be easily implemented on the real scanner systems since we purposefully constrain the optimization to produce realizable waveforms, and the gradients commonly available on MR systems can readily oscillate at frequencies of the order of kilohertz [7,17].

Future work will look at more complex models e.g. tissue models which more closely resemble the white matter tissue by including varying radius and fibre orientation inside each voxel. For those models we may see changes in the optimised GEN sequence and hence in the best choice of parametrised waveforms.

References

[1] P.T. Callaghan, A. Coy, T.P.J. Halpin, D. MacGowan, K.J. Packer, F.O. Zelaya, The Journal of Chemical Physics 97 (1992) 651.

[2] A. Coy, P.T. Callaghan, Journal of Colloid and Interface Science 168 (1994) 373–379.
[3] P.T. Callaghan, K.W. Jolley, J. Lelievre, Biophysical Journal 28 (1979) 133–141.
[4] S. Umbach, E. Davis, J. Gordon, P. Callaghan, Cereal Chemistry 69 (1992) 637.
[5] G.J. Stanisz, A. Szafer, G.A. Wright, R.M. Henkelman, Magnetic Resonance in Medicine 37 (1997) 103–111.
[6] Y. Assaf, T. Blumenfeld-Katzir, Y. Yovel, P.J. Basser, Magnetic Resonance in Medicine 59 (2008) 1347–1354.
[7] J. Xu, M. Does, J. Gore, Magnetic resonance in Medicine 61 (2009) 828–833.
[8] J. Piven, J. Bailey, B.J. Ranson, S. Arndt, American Journal of Psychiatry 154 (1997) 1051–1056.
[9] J.R. Hughes, Epilepsy and Behavior 11 (2007) 20–24.
[10] D.C. Alexander, Magnetic Resonance in Medicine 60 (2008) 439–448.
[11] I. Drobnjak, B. Siow, D.C. Alexander, Journal of Magnetic Resonance 206 (2010) 41–51.
[12] P.T. Callaghan, J. Stepisnik, Journal of Magnetic Resonance, Series A 117 (1995) 118–122.
[13] I. Drobnjak, D.C. Alexander, Journal of Magnetic Resonance 212 (2011) 344–354.
[14] P.T. Callaghan, Journal of Magnetic Resonance 129 (1997) 74–84.
[15] I. Drobnjak, H. Zhang, M.G. Hall, D.C. Alexander, Journal of Magnetic Resonance 210 (2011) 151–157.
[16] A. Ianus, B. Siow, I. Drobnjak, H. Zhang, D.C. Alexander, Journal of Magnetic Resonance 227 (2013) 25–34.
[17] B. Siow, I. Drobnjak, M. Lythgoe, D.C. Alexander, Journal of Magnetic Resonance 214 (2012) 51–60.